

Corneal topography with high-speed swept source OCT in clinical examination

Karol Karnowski,^{1,3} Bartłomiej J. Kaluzny,^{2,3} Maciej Szkulmowski,¹
Michalina Gora,¹ and Maciej Wojtkowski^{1,*}

¹*Institute of Physics, Nicolaus Copernicus University, Grudziadzka 5, 87-100 Torun, Poland*

²*Department of Ophthalmology, Collegium Medicum, Nicolaus Copernicus University Curie-Skłodowskiej 9,
85-094 Bydgoszcz, Poland*

³*Authors contributed equally to this work*

**max@fizyka.umk.pl*

Abstract: We present the applicability of high-speed swept source (SS) optical coherence tomography (OCT) for quantitative evaluation of the corneal topography. A high-speed OCT device of 108,000 lines/s permits dense 3D imaging of the anterior segment within a time period of less than one fourth of second, minimizing the influence of motion artifacts on final images and topographic analysis. The swept laser performance was specially adapted to meet imaging depth requirements. For the first time to our knowledge the results of a quantitative corneal analysis based on SS OCT for clinical pathologies such as keratoconus, a cornea with superficial postinfectious scar, and a cornea 5 months after penetrating keratoplasty are presented. Additionally, a comparison with widely used commercial systems, a Placido-based topographer and a Scheimpflug imaging-based topographer, is demonstrated.

© 2011 Optical Society of America

OCIS codes: (170.4500) Optical coherence tomography; (170.3880) Medical and biological imaging; (170.4470) Ophthalmology

References and links

1. J. A. Izatt, M. R. Hee, E. A. Swanson, C. P. Lin, D. Huang, J. S. Schuman, C. A. Puliafito, and J. G. Fujimoto, "Micrometer-scale resolution imaging of the anterior eye in vivo with optical coherence tomography," *Arch. Ophthalmol.* **112**(12), 1584–1589 (1994).
2. D. Huang, E. A. Swanson, C. P. Lin, J. S. Schuman, W. G. Stinson, W. Chang, M. R. Hee, T. Flotte, K. Gregory, C. A. Puliafito, and J. G. Fujimoto, "Optical coherence tomography," *Science* **254**(5035), 1178–1181 (1991).
3. M. J. Maldonado, L. Ruiz-Oblitas, J. M. Munuera, D. Aliseda, A. García-Layana, and J. Moreno-Montañés, "Optical coherence tomography evaluation of the corneal cap and stromal bed features after laser in situ keratomileusis for high myopia and astigmatism," *Ophthalmology* **107**(1), 81–87, discussion 88 (2000).
4. H. Hoerauf, C. Wirbelauer, C. Scholz, R. Engelhardt, P. Koch, H. Laqua, and R. Birngruber, "Slit-lamp-adapted optical coherence tomography of the anterior segment," *Graefes Arch. Clin. Exp. Ophthalmol.* **238**(1), 8–18 (2000).
5. M. Wojtkowski, R. Leitgeb, A. Kowalczyk, T. Bajraszewski, and A. F. Fercher, "In vivo human retinal imaging by Fourier domain optical coherence tomography," *J. Biomed. Opt.* **7**(3), 457–463 (2002).
6. A. F. Fercher, C. K. Hitzenberger, G. Kamp, and S. Y. El-Zaiat, "Measurement of intraocular distances by backscattering spectral interferometry," *Opt. Commun.* **117**(1-2), 43–48 (1995).
7. G. Häusler and M. W. Lindner, "'Coherence Radar' and 'Spectral Radar'—new tools for dermatological diagnosis," *J. Biomed. Opt.* **3**(1), 21–31 (1998).
8. M. Wojtkowski, V. Srinivasan, J. G. Fujimoto, T. Ko, J. S. Schuman, A. Kowalczyk, and J. S. Duker, "Three-dimensional retinal imaging with high-speed ultrahigh-resolution optical coherence tomography," *Ophthalmology* **112**(10), 1734–1746 (2005).
9. R. Leitgeb, C. Hitzenberger, and A. Fercher, "Performance of fourier domain vs. time domain optical coherence tomography," *Opt. Express* **11**(8), 889–894 (2003).
10. M. Wojtkowski, V. Srinivasan, T. Ko, J. Fujimoto, A. Kowalczyk, and J. Duker, "Ultrahigh-resolution, high-speed, Fourier domain optical coherence tomography and methods for dispersion compensation," *Opt. Express* **12**(11), 2404–2422 (2004).

11. J. F. de Boer, B. Cense, B. H. Park, M. C. Pierce, G. J. Tearney, and B. E. Bouma, "Improved signal-to-noise ratio in spectral-domain compared with time-domain optical coherence tomography," *Opt. Lett.* **28**(21), 2067–2069 (2003).
12. S. Radhakrishnan, A. M. Rollins, J. E. Roth, S. Yazdanfar, V. Westphal, D. S. Bardenstein, and J. A. Izatt, "Real-time optical coherence tomography of the anterior segment at 1310 nm," *Arch. Ophthalmol.* **119**(8), 1179–1185 (2001).
13. C. K. S. Leung, W.-M. Chan, C. Y. Ko, S. I. Chui, J. Woo, M.-K. Tsang, and R. K. K. Tse, "Visualization of anterior chamber angle dynamics using optical coherence tomography," *Ophthalmology* **112**(6), 980–984 (2005).
14. G. Baikoff, E. Lutun, C. Ferraz, and J. Wei, "Static and dynamic analysis of the anterior segment with optical coherence tomography," *J. Cataract Refract. Surg.* **30**(9), 1843–1850 (2004).
15. B. J. Kaluzny, J. J. Kaluzny, A. Szkulmowska, I. Gorczyńska, M. Szkulmowski, T. Bajraszewski, M. Wojtkowski, and P. Targowski, "Spectral optical coherence tomography: a novel technique for cornea imaging," *Cornea* **25**(8), 960–965 (2006).
16. I. Grulkowski, M. Gora, M. Szkulmowski, I. Gorczynska, D. Szlag, S. Marcos, A. Kowalczyk, and M. Wojtkowski, "Anterior segment imaging with Spectral OCT system using a high-speed CMOS camera," *Opt. Express* **17**(6), 4842–4858 (2009).
17. S. H. Yun, G. Tearney, J. de Boer, and B. Bouma, "Motion artifacts in optical coherence tomography with frequency-domain ranging," *Opt. Express* **12**(13), 2977–2998 (2004).
18. T. Bajraszewski, M. Wojtkowski, M. Szkulmowski, A. Szkulmowska, R. Huber, and A. Kowalczyk, "Improved spectral optical coherence tomography using optical frequency comb," *Opt. Express* **16**(6), 4163–4176 (2008).
19. M. Wojtkowski, "High-speed optical coherence tomography: basics and applications," *Appl. Opt.* **49**(16), D30–D61 (2010).
20. M. Choma, M. Sarunic, C. Yang, and J. Izatt, "Sensitivity advantage of swept source and Fourier domain optical coherence tomography," *Opt. Express* **11**(18), 2183–2189 (2003).
21. S. Yun, G. Tearney, J. de Boer, N. Iftimia, and B. Bouma, "High-speed optical frequency-domain imaging," *Opt. Express* **11**(22), 2953–2963 (2003).
22. W. Y. Oh, S. H. Yun, G. J. Tearney, and B. E. Bouma, "115 kHz tuning repetition rate ultrahigh-speed wavelength-swept semiconductor laser," *Opt. Lett.* **30**(23), 3159–3161 (2005).
23. M. K. Leung, A. Mariampillai, B. A. Standish, K. K. C. Lee, N. R. Munce, I. A. Vitkin, and V. X. D. Yang, "High-power wavelength-swept laser in Littman telescope-less polygon filter and dual-amplifier configuration for multichannel optical coherence tomography," *Opt. Lett.* **34**(18), 2814–2816 (2009).
24. M. A. Choma, K. Hsu, and J. A. Izatt, "Swept source optical coherence tomography using an all-fiber 1300-nm ring laser source," *J. Biomed. Opt.* **10**(4), 044009 (2005).
25. R. Huber, M. Wojtkowski, K. Taira, J. Fujimoto, and K. Hsu, "Amplified, frequency swept lasers for frequency domain reflectometry and OCT imaging: design and scaling principles," *Opt. Express* **13**(9), 3513–3528 (2005).
26. R. Huber, M. Wojtkowski, and J. G. Fujimoto, "Fourier Domain Mode Locking (FDML): A new laser operating regime and applications for optical coherence tomography," *Opt. Express* **14**(8), 3225–3237 (2006).
27. C. M. Eigenwillig, W. Wieser, B. R. Biedermann, and R. Huber, "Subharmonic Fourier domain mode locking," *Opt. Lett.* **34**(6), 725–727 (2009).
28. R. Huber, D. C. Adler, and J. G. Fujimoto, "Buffered Fourier domain mode locking: Unidirectional swept laser sources for optical coherence tomography imaging at 370,000 lines/s," *Opt. Lett.* **31**(20), 2975–2977 (2006).
29. S. D. Klyce, "Computer-assisted corneal topography. High-resolution graphic presentation and analysis of keratoscopy," *Invest. Ophthalmol. Vis. Sci.* **25**(12), 1426–1435 (1984).
30. C. Roberts, "Corneal topography: a review of terms and concepts," *J. Cataract Refract. Surg.* **22**(5), 624–629 (1996).
31. M. W. Belin and S. S. Khachikian, "An introduction to understanding elevation-based topography: how elevation data are displayed - a review," *Clin. Experiment. Ophthalmol.* **37**(1), 14–29 (2009).
32. G. Savini, P. Barboni, M. Carbonelli, and K. J. Hoffer, "Agreement between Pentacam and videokeratography in corneal power assessment," *J. Refract. Surg.* **25**(6), 534–538 (2009).
33. M. Gora, K. Karnowski, M. Szkulmowski, B. J. Kaluzny, R. Huber, A. Kowalczyk, and M. Wojtkowski, "Ultra high-speed swept source OCT imaging of the anterior segment of human eye at 200 kHz with adjustable imaging range," *Opt. Express* **17**(17), 14880–14894 (2009).
34. American National Standards Institute, "American National Standard for Safe Use of Lasers," ANSI Z136.1 (2007).
35. S. Ortiz, D. Siedlecki, L. Remon, and S. Marcos, "Optical coherence tomography for quantitative surface topography," *Appl. Opt.* **48**(35), 6708–6715 (2009).
36. S. Ortiz, D. Siedlecki, I. Grulkowski, L. Remon, D. Pascual, M. Wojtkowski, and S. Marcos, "Optical distortion correction in optical coherence tomography for quantitative ocular anterior segment by three-dimensional imaging," *Opt. Express* **18**(3), 2782–2796 (2010).
37. D. Z. Reinstejn, T. J. Archer, and M. Gobbe, "Corneal epithelial thickness profile in the diagnosis of keratoconus," *J. Refract. Surg.* **25**(7), 604–610 (2009).

1. Introduction

Anterior segment optical coherence tomography (OCT) was introduced in 1994 [1]. It was based on a time domain OCT method presented three years earlier, in which the distribution of scattering points along the scanning beam is detected indirectly by varying the length of the reference arm of the Michelson interferometer [2]. The first commercial time domain OCT instrument, called OCT1 (produced by Humphrey Instruments, Inc., later acquired by Carl Zeiss, Inc.), used a light source with central wavelength of 830 nm and was designed to measure the human retina. After some modifications, it was possible to reconstruct cross-sectional images of only a small portion of the anterior segment, with an imaging speed of 100–400 lines/s [3]. Results from a prototype, based on 1310 nm superluminescent diode capable of covering larger portion of the anterior segment—entire cross-sectional information about the cornea—were reported in 2000 [4], and 5 years later a commercial 1310 time domain OCT system for anterior segment imaging was launched under the name Visante OCT (Carl Zeiss, Inc.). Currently this is the most widely used OCT device for dedicated *in vivo* anterior segment imaging. It provides cross-sectional images with axial resolution of 18 μm and an imaging speed of 2000 lines/s. Visante OCT creates pachymetry maps but cannot perform topographic analysis of the cornea, mostly because of limitations in acquisition time. The introduction of Fourier domain OCT in 2002 [5–7], with the primary advantage of increased sensitivity or speed and the possibility of three-dimensional imaging [8–11], promised to improve the ability of OCT to quantitatively assess the corneal topography [12–16]. Although commercial Fourier domain OCT systems using a spectrometer (Spectral OCT –SOCT) have reached an axial resolution of 3–6 μm and imaging speed of 20,000–50,000 lines/s, they are not able to provide adequate assessment of anterior and posterior corneal topography because of significantly strong fringe washout and sensitivity drop off typical for SOCT [17–19].

High-speed swept source OCT (SS OCT), first reported in 2003, employs wavelength tunable lasers (and is a promising new modality for quantitative evaluation of the cornea. SS OCT provides improved imaging speed and higher sensitivity in comparison with previous OCT technologies [20]. Two major modalities, depending on the method used for wavelength selection, can be used here: diffraction grating with polygonal mirror [21–23] or fiber Fabry-Perot tunable filter [24,25]. SS OCT performance might be additionally improved by Fourier domain mode locking (FDML) lasers achieving a repetition rate of up to several hundreds of kilohertz [26–28]. Apart from improved speed and sensitivity, there is another advantage of 1300 nm SS OCT for anterior segment imaging, due to its better tissue penetration for the central wavelength comparing with 800 nm light sources, especially for those applications when iris, sclera, or irido-scleral angle are investigated. Recently, Tomey Corporation (Japan) introduced an instrument for anterior segment evaluation based on SS OCT. It offers an axial resolution of 10 μm and a scanning speed of 30,000 lines/s, which is equivalent to commercial SOCT instruments. One of the most important features of this system is the ability to provide topographic maps of both anterior and posterior surfaces of the cornea.

In current clinical and interventional ophthalmic practice, precise quantitative assessment of the cornea is more important than ever. Robust development in the field of refractive surgery has resulted in the need for very early diagnosis of corneal ectatic diseases, ideally at a subclinical stage. Knowledge of the exact corneal shape is essential, not only to determine patients' suitability to undergo surgery, but also to properly plan the treatment. Placido-based computerized videokeratoscopy, proposed first by Klyce in 1984 [29], is incapable of providing all required information. In this technology, multiple concentric light rings are projected onto the cornea. The reflected image is captured on a camera, and computer software analyzes the data and displays the results. The deviation of reflected rings is measured, and the curvature of the corneal surface points in the axial direction is calculated, primarily. Surface curvature measures how fast the surface bends at a certain point in a certain

direction. The error of Placido-based corneal topography under optimal conditions is ± 0.25 D, but in abnormal corneas seen in clinical practice it is often ± 0.50 – 1.00 D [30]. This technology has several inherent limitations:

- There is no information on the posterior corneal surface, but many ectatic disorders initially present changes posteriorly.
- Pachymetric maps depicting the distribution of corneal thickness cannot be made.
- The imaging requires an intact epithelial surface and healthy tear film.
- The data over the apex of the cornea and the periphery are commonly extrapolated from the surrounding curvature.

Recently introduced elevation-based topography overcomes the shortcomings of Placido-based systems. True topographic imaging requires the reconstruction of the corneal image in three dimensions [31]. It is very difficult to detect pattern differences on a map produced with raw elevation data; thus a reference shape must be used. The most commonly used is the best-fit sphere (BFS), but the best fit ellipse and the best fit toric ellipsoid can also be used. The elevation of a point on the corneal surface is displayed as the height of the point on the corneal surface relative to a spherical reference surface. The best fit sphere is calculated by dedicated software for every elevation map separately.

At the moment, four systems use optical cross sectioning to triangulate both the anterior and the posterior corneal surfaces. Orbscan (Bausch & Lomb, USA) uses a scanning-slit technology, and Pentacam (OCULUS, Germany), Galilei (Ziemer, Switzerland), and TMS-5 (Tomey, Japan) utilize rotating Scheimpflug imaging. Although the instruments based on rotating Scheimpflug cameras are considered the most comprehensive and accurate, they also have some limitations. The most important is the imaging speed. Pentacam requires 2.0 seconds to obtain 50 radial scans. This increases the risk of motion artifacts, even though there is an inbuilt second camera to control for eye movements. Moreover, radial scanning may not provide sufficient scan density of the corneal periphery, resulting in a requirement for interpolation. Another limitation is that the instruments using the Scheimpflug principle are less accurate in comparison to Placido-based ones in providing traditional curvature maps of the anterior surface, and only moderate agreement in simulated keratometry values between these technologies are reported [32]. Also, from the perspective of using different OCT techniques, we must consider the speed as one of the most important factors. Reasonably high corneal curvature leads to strong signal drop in spectrometer-based OCT or to a resolution decrease in SS OCT due to the fringe washout effect [17]. To avoid this drawback, dense transverse scanning is required, and the same applies to higher speed OCT systems. Another reason for choosing a SS OCT instrument for corneal topography is the much less profound effect of depth dependent signal decay in SS OCT comparing with spectrometer-based systems [33].

The aim of this paper is to present the applicability of a next-generation system using a swept laser working with a repetition rate of 108,000 lines/s, along with OCT technology, for quantitative evaluation of the cornea. The first elevations maps generated with a SS OCT setup have been already presented [33]. However, no deeper analysis and verification of published results, especially for eyes with pathologies, has been presented so far. Here we would like to perform such preliminary verification by comparing the performance of the prototype SS OCT system with currently used technologies: Placido-based topography and Scheimpflug imaging-based topography. According to our best knowledge, this is the first study presenting SS-OCT-based quantitative analysis of the anterior segment for different clinical pathologies in comparison with commercial systems.

2. Swept-source-based system for corneal topography

Figure 1 shows the experimental setup of the SS OCT system with a 1300 nm FDML laser operating as a light source, both constructed in the Institute of Physics at Nicolaus Copernicus University, Torun, Poland. Details of the design of the SS OCT instrument are given elsewhere [33]. For the purpose of this study, two changes in laser operation were introduced: the frequency of the Fabry-Perot filter driving signal was set to 54 kHz (108 kHz effective sweep rate), and a filter scanning range of 82 nm (Fig. 1a) was chosen—resulting in 20 μm of axial resolution in tissue and an imaging depth of 9 mm. These are necessary settings to get information about corneal surfaces and the iris. The average output power of the FDML laser was 21 mW. The eye was illuminated with 2.5 mW of optical power, which is consistent with safety exposure limits for the human eye given by the American National Standards Institute (ANSI) [34]. The system sensitivity was measured to be 105 dB at 9.2 μs exposure time. To generate the reference fringe pattern for numerical recalibration to the optical frequency space, a silica glass plate was used. This approach is an alternative to using a Michelson or Mach-Zehnder interferometer. Because of the very low dispersion of silica at 1300 nm, the interference between glass surfaces produces more stable fringes and provides an invariable parameter for conversion to real geometry in the z -axis.

The SS OCT system presented here uses a scanning protocol of 50 B-scans with 500 A-scans each. Such a raster scanning was selected in order to obtain dense 3D information of corneal topography and to minimize artifacts caused by involuntary eye movements. A single tomogram was measured within 4.6 ms. Each 3D volume was captured within 230 ms. The lateral dimension of the scanned area was 11.2 mm \times 11.2 mm.

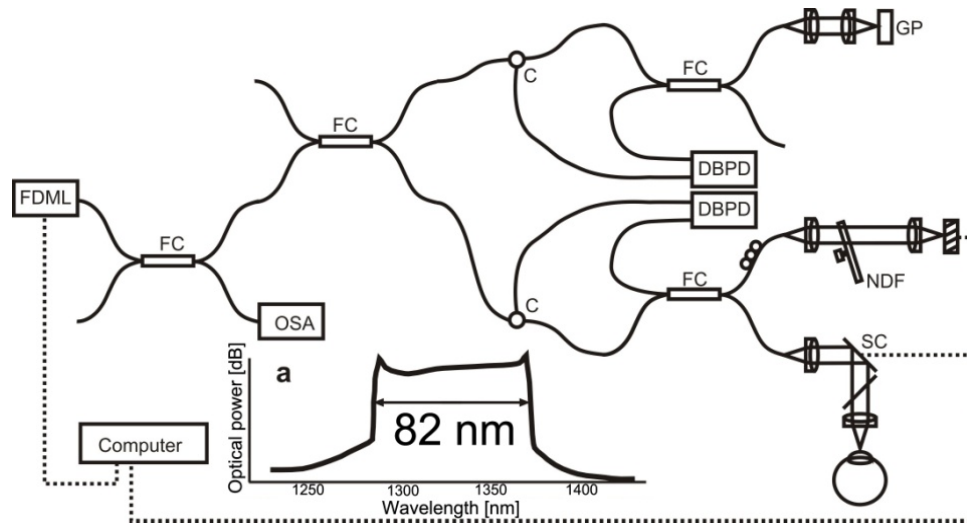


Fig. 1. Diagram of SS OCT setup for anterior segment imaging (FMDL, swept laser with optical delay line; OSA, optical spectrum analyzer; FC, fiber coupler; C, circulator; DBPD, dual-balanced photo diode; NDF, neutral density filter; GP, glass plate; GS, xy galvo scanners. (a) Optical spectrum of FDML laser constructed at Nicolaus Copernicus University.

Collected data were postprocessed (k-space resampling, shaping, and fast Fourier transformation) to achieve cross-sectional images. The segmentation procedure was employed to delineate the corneal surfaces and mark pupil edges. Segmented data were corrected for index of refraction and tilt misalignment. At this level, topography maps of both cornea surfaces as well as cornea thickness were calculated. Subsequently, the sphere was fitted (best-fit sphere) to anterior and posterior cornea surfaces, and differences between the fitted surface and real data were plotted on elevation maps. Supplementary to measurements performed by a prototype SS OCT system, two other standard instruments were used: a

conventional Placido-based topographer (PTC 110, Optopol Technology, Poland) and a rotating Scheimpflug camera (Pentacam HR, Oculus, Germany). We used sagittal (axial) anterior surface maps from the Placido-based topographer and elevation subtraction maps created with the use of the best-fit sphere algorithm (BFS). It should be mentioned here that Scheimpflug images were processed (segmentation, fitting, calculating for elevation maps) with software provided by the manufacturer. For elevation-based systems, the same color scales and the same 9 mm area of interest were used. All examinations of the same patient were performed in a single day in a noninvasive, noncontact manner.

Written informed consent was obtained from all patients. The Ethics Committee of the Collegium Medicum in Bydgoszcz, Nicolaus Copernicus University in Torun, Poland, approved the study.

3. Results and discussion

Fan and optical distortions can significantly affect image reconstruction in OCT cross-sectional images, and the same can strongly obstruct corneal topographic reconstruction. The fan distortion is associated with the OCT scanning system, which includes a pair of separate scanner mirrors and optical elements. Optical distortions are related to imaging optics and can cause, for example, pincushion or barrel effects in projection OCT images. When flat surfaces are imaged with OCT, they become curved. However, this effect can be minimized by careful adjustment of the optical setup. Following Ortiz *et al.* [35,36], we have adjusted the position of the objective lens with respect to scanners to decrease the magnitude of fan distortion. During this procedure a flat surface was imaged on a screen in the preview mode in two orthogonal directions. Careful adjustment of the objective lens position enabled us to flatten reconstructed images, which are presented in Figs. 2a and 2b for two perpendicular directions. To investigate the influence of fan and optical distortion of our OCT system in three dimensions, we performed a simple experiment using 2D gridlines printed on paper, which

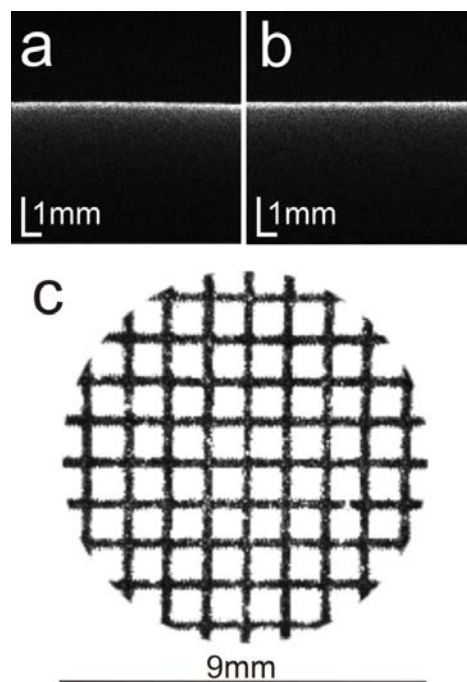


Fig. 2. SS OCT images of a flat surface measured in two perpendicular directions, (a) horizontally and (b) vertically, after optical distortion correction. (c) *En face* projection image from 3-D OCT data for graph paper in a 9 mm \times 9 mm area.

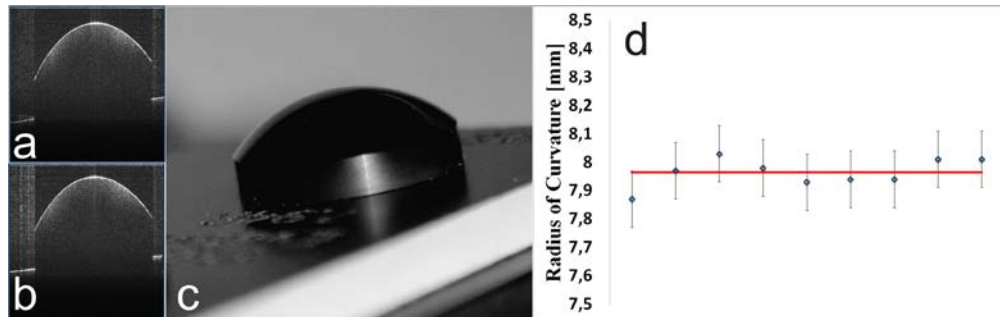


Fig. 3. (a–b) central OCT images of the reference sphere; (c) photograph of the reference sphere with 7.94 mm radius of curvature. (d) Radius of curvature for nine different OCT measurements; diamonds, mean value; red line, radius given by manufacturer.

were then measured by the SS OCT system. Figure 2c shows an *en face* projection image generated from 3D OCT data. The view is limited to the 9 mm area (the same area size used for elevation map calculation). A slight defocusing is visible at the edge of the scanned area. However, the shape of the grid is not significantly distorted. We can assume that for demonstration of the applicability of SSOCT for corneal topography the optical distortions are negligible.

To verify the performance of the SS OCT system for anterior segment imaging, a reference sphere was measured (EyeSys Technologies) (Fig. 3c). The reference sphere was measured at nine different randomly set tilt-shift positions (Figs. 3a–3b), which was consistent with the scanning protocol used for patient examination. Since the reference sphere consists only of one surface, the postprocessing was performed without the refraction correction step. The reference shape was segmented automatically by using custom designed software written in LabView. In the method proposed by Gora *et al.* [33] the pupillary plane is used for mathematical correction of tilt or misalignment of the measured eye with respect to the optical axis of the instrument. As the reference sphere has no pupil, we used the basal surface of the target.

For each of nine measurements the best fit sphere was found, and its radius of curvature was calculated (Fig. 3d). A mean value of 7.96 mm (standard deviation of 0.07 mm) was consistent with the value given by the manufacturer of the reference sphere (7.94 mm) and the value measured by the Placido-based topographer (7.94 mm). The 0.07 mm error for a 7.96 mm radius will produce a 0.37 D error.

Quantitative analysis of three corneas from three different patients (keratoconus, a cornea with superficial postinfectious scar, and a cornea 5 months after penetrating keratoplasty) was performed with three different instruments. Figure 4 shows the topographic analysis of a keratoconic cornea measured with three different instruments. The confirmation of the clinically significant keratoconus is based on Placido topography in which typical pattern is detected on anterior sagittal curvature map. We revealed good agreement between anterior elevation topographies provided by Pentacam and SS OCT in this case (Fig. 4). The central keratometry value (K1) and axis in a flat meridian is almost the same for Placido-based topography, Pentacam, and SS OCT, but readings for a steep meridian (K2) show differences above 1 D and above 20° between the Placido-based topographer and elevation-based systems (Table 1). Agreement of the results from elevation topographers is also high for posterior corneal topography and pachymetry.

Figure 5 shows results of the examination of the cornea with a scar in the anterior stroma after superficial infectious ulcer. Placido topography shows irregular astigmatism, and keratometric values are quite different from elevation-based systems. Pentacam shows an area below the reference shape in the center and paracentrally, whereas SS OCT topography shows


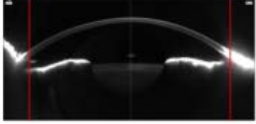
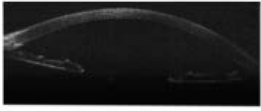
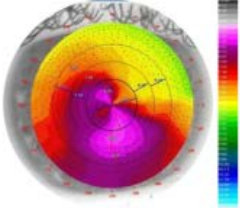
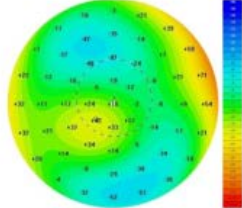
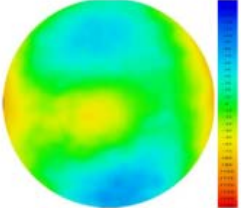
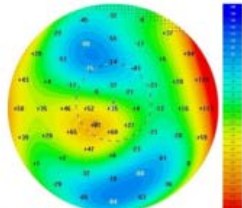
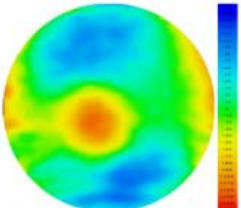
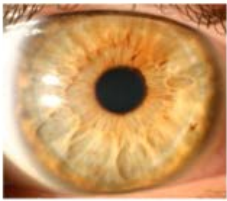
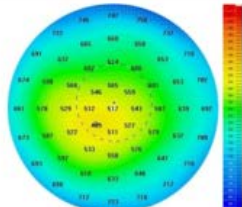
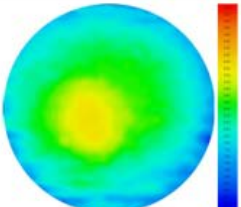
	Placido topography	Scheimpflug camera	SS OCT tomography
Source data			
Anterior surface			
K1 (ax) K2 (ax)	7.38 mm 45.73 D (15°) 6.33 mm 53.30 D (110°)	7.47 mm 45.2 D (32.6°) 6.51 mm 51.9 D (122.6°)	7.41 mm 45.6 D (35.5°) 6.59 mm 51.2 D (141.2°)
Posterior surface			
K1 (ax) K2 (ax)		6.08 mm -6.6 D (24.7°) 5.02 mm -8.0 D (114.7°)	6.07 mm -6.6 D (24.7°) 5.6 mm -7.2 D (116.5°)
Slit-lamp photo/ <u>Pachymetry</u>			
Min. thickness		499 μm	492 μm

Fig. 4. Qualitative evaluation of a keratoconic cornea with three different instruments. K1, K2, central keratometry readings. The red lines on Scheimpflug images correspond to the lateral size of cross-sectional images for SS OCT.

a more regular anterior surface. Posterior topography patterns are similar for both instruments; thus a distinct decrease of corneal thickness in the center is visible on Pentacam pachymetry map compared with that calculated by the SS OCT system (Table 1).

Figures 6(a–b) show magnified tomograms of the cornea with a scar measured with the Pentacam HR and the SS OCT prototype. Blue light from the 475 nm LED of the Pentacam imaging system is strongly reflected back from the opaque scarring tissue. The signal is oversaturated, which results in difficulties in segmentation of the anterior surface. Moreover, the posterior surface delineation is poor. In contrast to SS OCT, Pentacam segmentation causes a falsely decreased thickness of the central cornea (Fig. 6a). On SS OCT images, both anterior and posterior surfaces are clearly visible and easy to delineate. In addition, because of its better resolution and sensitivity, SS OCT offers a much better view of the corneal structure.

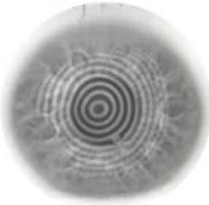
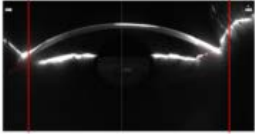
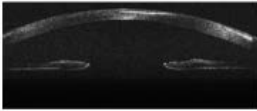
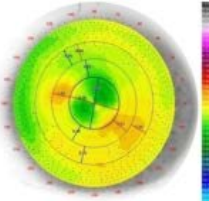
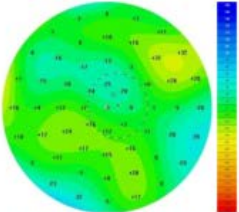
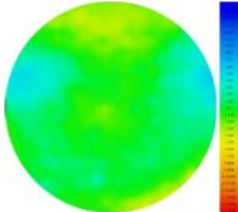
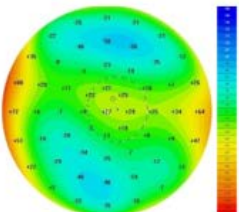
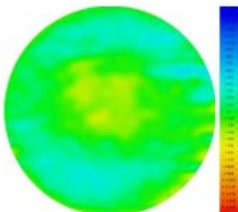

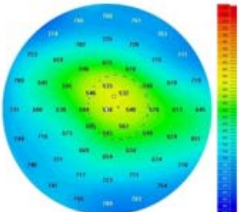
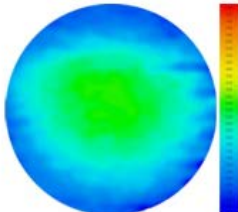
	Placido topography	Scheimpflug camera	SS OCT tomography
Source data			
Anterior surface			
K1 (ax) K2 (ax)	8.67 mm 38, 93.1 D (80°) 8.20 mm 41.17 D (165°)	9.09 mm 37.1 D (29.5°) 8.37 mm 40.3 D (119.5°)	8.61 mm 39.2 D (166°) 7.91 mm 42.7 D (76°)
Posterior surface			
K1 (ax) K2 (ax)		6.22 mm -6.4 D (159.9°) 5.6 mm -7.1 (69.9°)	7.15 mm -5.6 D (120°) 6.76mm -6.0 D (30°)
Slit-lamp photo/ <u>Pachymetry</u>			
Min. thickness		523 μm	591 μm

Fig. 5. Qualitative evaluation of a cornea with superficial postinfectious scar with three different instruments. K1, K2, central keratometry readings. The red lines on Scheimpflug images correspond to the lateral size of cross-sectional images for SS OCT.

In this pathological case, SS OCT images reveal that the lack of superficial stromal tissue due to the scarring process is compensated by increased thickness of the epithelium (Fig. 6(b)), and the resultant corneal thickness is larger than that measured by the Pentacam instrument (Table 1).

Results obtained from the eye 5 months after penetrating keratoplasty are shown in Fig. 7. Placido reflections are much distorted. Only a couple of rings in the center could be partially distinguished and analyzed by the computer. Despite the fact that part of the cornea is covered with the upper lid, the Placido system provides a curvature map of the whole cornea.

Also, the differences in the central keratometry reading are very large in comparison with Pentacam and SS OCT. Anterior topographies from Pentacam and SS OCT show comparable patterns, but the elevated central island is located slightly higher on the SS OCT map, resulting in a significant difference in central keratometry readings.

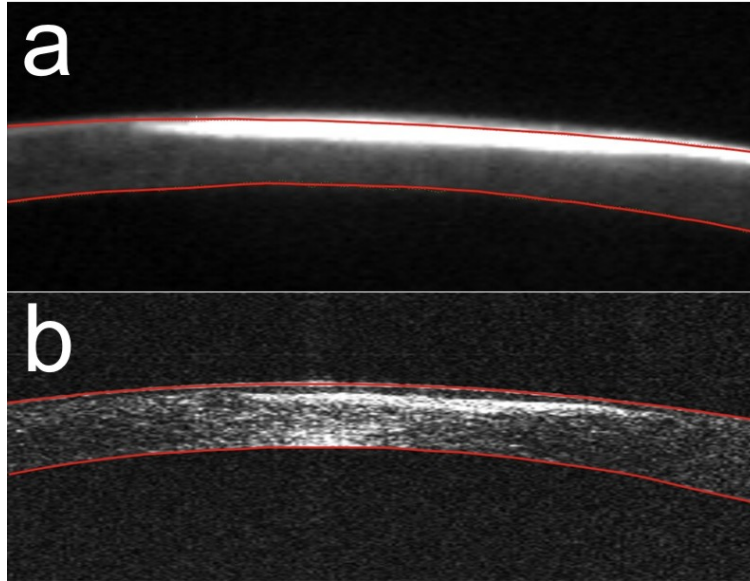


Fig. 6. Cross-sectional images of the cornea with superficial postinfectious scar: (a) Scheimpflug image measured by Pentacam HR; (b) SS OCT cross-sectional image. Red lines delineate the segmented corneal boundaries.

The area where the donor and host tissues are interconnected is more elevated on maps generated with SS OCT. As a result, SS OCT shows much thicker pachymetry in the area of graft-host junction.

A closer look on a single cross-sectional image has to be done to fully understand origin of differences in elevation maps generated with both Pentacam and SS OCT.

Figure 8 shows tomograms of the corresponding parts of the cornea after penetrating keratoplasty acquired with two different instruments. The Scheimpflug image is moderately clear, and segmentation of the tissue by the software is not correct (Fig. 8(a)). This inaccuracy is caused by the simplified segmentation algorithm's assuming a certain level of corneal smoothness, which is obviously not true in the case of very complex corneal topography like that after penetrating keratoplasty. SS OCT provides tomograms with a more homogenous distribution of the backscattered intensity. Therefore it is easier to apply a segmentation algorithm that does not assume the smoothness of the corneal surface (Fig. 8(b)).

4. Conclusions

In this paper, we demonstrated the applicability of the high-speed SS OCT system for quantitative evaluation of the cornea. Full 3D anterior segment imaging necessary to perform further topographic analysis was achieved with the custom-designed SS OCT system running with speed of 108,000 lines/s, 20 μm axial resolution in tissue, and imaging depth of 9 mm. A raster scanning protocol with 25000 lateral points was applied to obtain better coverage of the cornea. Dense sampling is especially important in cases with focal pathologic changes. The accuracy of keratometry readings was verified on the reference sphere from EyeSys Technologies, showing good correlation with values given by the manufacturer and high repeatability of measurements. Quantitative analysis of corneas with pathological changes was performed with three different instruments: the SS OCT system, a Placido-based topographer, and a rotating Scheimpflug camera system.

In conclusion, high-speed SS OCT is a promising technology for quantitative corneal evaluation that has some advantages over the Scheimpflug system, including better tomogram quality and shorter measurement time. However, the most important advantage is that

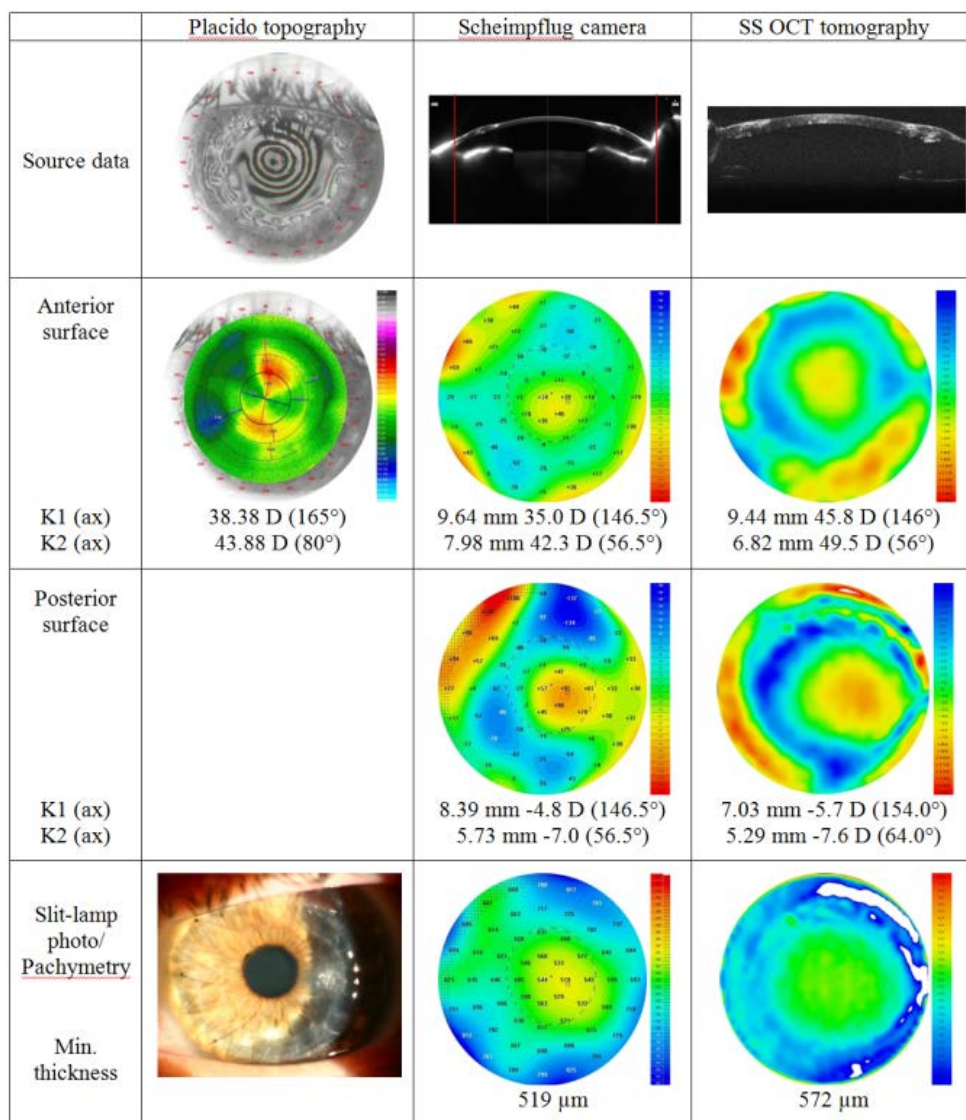


Fig. 7. Qualitative evaluation of a cornea 5 months after penetrating keratoplasty with three different instruments. K1, K2, central keratometry readings. The red lines on Scheimpflug images correspond to the lateral size of cross-sectional images from SS OCT.

topographic analysis can be done along with the high-quality cross-sectional imaging. SS OCT could be used not only for elevation-based topography but also for evaluation of the corneal structure, including the epithelium. Thus, as a decrease in epithelial thickness masks the presence of an underlying cone on front surface topography [37], SS OCT may be helpful in detecting keratoconus at a very early stage.

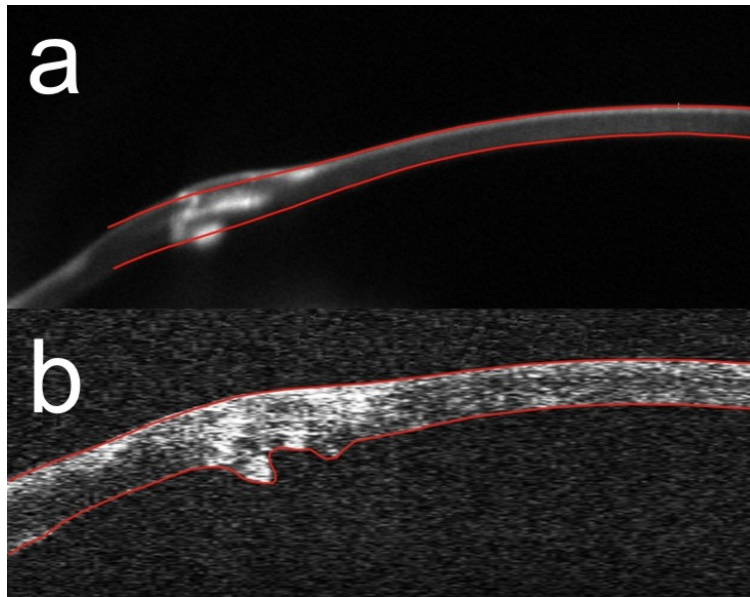


Fig. 8. Cross-sectional images of the cornea after penetrating keratoplasty: (a) Scheimpflug image measured by Pentacam HR, (b) SS OCT cross-sectional image. Red lines delineate the segmented corneal boundaries.

Table 1. Central keratometry readings and central thickness for selected corneal pathologies; all patients measured with three different instruments

	Pladico topography	Scheimpflug camera	SSOCT tomography
Keratoconic cornea			
Anterior K1 (ax)	7.38 mm 45.73 D (15°)	7.47 mm 45.2 D (32.6°)	7.41 mm 45.6 D (35.5°)
Anterior K2 (ax)	6.33 mm 53.30 D (110°)	6.51 mm 51.9 D (122.6°)	6.59 mm 51.2 D (141.2°)
Posterior K1 (ax)	—	6.08 mm -6.6 D (24.7°)	6.07 mm -6.6 D (24.7°)
Posterior K2 (ax)	—	5.02 mm -8.0 D (114.7°)	5.6 mm -7.2 D (116.5°)
Central thickness	—	499 μ m	492 μ m
Cornea with postinfectious scar			
Anterior K1 (ax)	8.67 mm 38,93.1 D (80°)	9.09 mm 37.1 D (29.5°)	8.61 mm 39.2 D (166°)
Anterior K2 (ax)	8.20 mm 41.17 D (165°)	8.37 mm 40.3 D (119.5°)	7.91 mm 42.7 D (76°)
Posterior K1 (ax)	—	6.22 mm -6.4 D (159.9°)	7.15 mm -5.6 D (120°)
Posterior K2 (ax)	—	5.6 mm -7.1 (69.9°)	6.76mm -6.0 D (30°)
Central thickness	—	523 μ m	591 μ m
Cornea after 5 penetrating keratoplasties			
Anterior K1 (ax)	38.38 D (165°)	9.64 mm 35.0 D (146.5°)	9.44 mm 45.8 D (146°)
Anterior K2 (ax)	43.88 D (80°)	7.98 mm 42.3 D (56.5°)	6.82 mm 49.5 D (56°)
Posterior K1 (ax)	—	8.39 mm -4.8 D (146.5°)	7.03 mm -5.7 D (154.0°)
Posterior K2 (ax)	—	5.73 mm -7.0 (56.5°)	5.29 mm -7.6 D (64.0°)
Central thickness	—	519 μ m	572 μ m

Acknowledgments

This work was supported by EuroHORCs-European Science Foundation EURYI Award EURYI-01/2008-PL (M. Wojtkowski) and Polish Ministry of Science and Higher Education Grant N N402 084435 (B. J. Kaluzny) Project was operated within the Foundation for Polish Science Ventures Programme co-financed by the EU European Regional Development Fund (M. Gora). K. Karnowski acknowledges support form Polish Ministry of Science and Higher Education Supervisor Grant N N402 482039.